ION KINETIC-ENERGY DISTRIBUTIONS AND ELECTRICAL MEASUREMENTS IN Ar/O_2 RF GLOW DISCHARGES

J. K. Olthoff, R. J. Van Brunt, and M. A. Sobolewski

National Institute of Standards and Technology, Gaithersburg, MD 20899 USA

INTRODUCTION

Low-pressure rf glow discharges of electronegative gases are widely used in the etching of thin films. These gases form negative ions by electron capture that influence the physical properties of glow discharges. However, because the negative ions are trapped by the positive potential of the bulk plasma, direct detection is difficult [1]. This experimental difficulty has limited the number of investigations related to negative ions in rf glow discharges, thus preventing a thorough understanding of the role of negative ions in etching plasmas.

As an alternative to the direct detection of negative ions, we have undertaken a study of the effects of negative ions on various plasma parameters. Previous measurements have shown that the addition of small amounts of an electronegative gas to an argon plasma causes substantial changes in the kinetic-energy distributions of Ar^+ ions sampled from the discharge [2]. We have utilized a mass spectrometer with an ion energy analyzer to systematically investigate the effects of varying the oxygen concentration in an argon/oxygen discharge on the kinetic energies of positive ions sampled from the plasma. Analysis of the trends in the distributions as the O_2 content is varied provides a more complete picture of the effects of an electronegative gas on the rf plasma characteristics. This type of investigation also has implications for understanding the effects of impurities in the etching process.

Kinetic-energy distributions for Ar^+, Ar_2^+, Ar^{++}, O_2^+, and O^+ ions sampled from argon/oxygen plasmas produced in a parallel plate rf reactor are presented. The oxygen content of the feed gas was varied from 0–20 % while the pressure and applied rf voltage were held constant. The effects of the varying oxygen content on the voltage and current waveforms across the plasma were also determined.

EXPERIMENTAL

All experiments were performed using a GEC* rf Reference Cell whose characteristics have been described elsewhere [3–5]. Briefly, the electrode configuration is symmetric, with two 10.2-cm diameter aluminum electrodes with an interelectrode spacing of 2.54 cm. RF power (at 13.56 MHz) is capacitively coupled to the lower electrode through a 0.1 μF blocking capacitor while the upper electrode is grounded. All experiments were performed using 99.999 % argon and 99.9 % oxygen supplied through a showerhead hole arrangement in the upper electrode. The feed gas mixtures were supplied from the output of two mass flow controllers. All data presented in this paper were obtained for a total pressure of 13.3 Pa and an *applied* rf voltage of 200 V (peak-to-peak).

*Gaseous Electronics Conference

The mass-spectrometer apparatus is a Vacuum Generators SXP300-CMA system [6] which consists of a cylindrical mirror ion-energy analyzer [7] coupled to a 300 AMU quadrupole mass spectrometer. Ions were sampled via a 200 μm aperture through a grounded stainless steel cone into the differentially pumped region of the analyzer. The ions were collected from the side of the plasma at a point in line with the edge of the electrodes and equidistant between the electrode faces.

Ion energy distributions were obtained by tuning the mass spectrometer to a particular mass and then scanning the energy of the ions entering the energy analyzer. An energy resolution of 0.5 eV was maintained over the entire energy range scanned. Corrections to the ion kinetic-energy scale for an energy shift caused by surface-charging effects in the sampling cone were made based upon the observed kinetic-energy threshold for Ar^+ from an argon discharge [8].

Voltage and current waveforms were measured at the base of the powered electrode using a 300 MHz digital oscilloscope and 200 MHz voltage and current probes. The Fourier components of the voltage and current across the plasma were then calculated using a simple circuit model to correct for the stray impedance of the discharge cell. The model, consisting of a single parasitic inductance in series with the plasma and a single parasitic capacitance in parallel, has been described in detail elsewhere [4].

RESULTS

Ion Kinetic-Energy Distributions

The kinetic-energy distributions for Ar^+ ions sampled from a range of argon/oxygen plasmas are presented in Fig. 1. For pure argon, the kinetic-energy distribution is similar to those published previously [2]. The broad distribution and the secondary maxima are a result of charge-exchange collisions that occur as the Ar^+ ions are accelerated from the bulk plasma to the grounded surface of the sampling cone [8–10]. When a small amount of oxygen (2 %) is added to the plasma, the maximum kinetic energy increases and the shape of the distribution changes for higher energy ions. These changes indicate modifications of the characteristics of the sheath. As the oxygen content increases beyond 2%, the maximum kinetic energy decreases, and a clear progression in the secondary maxima towards lower energies is observed.

Figure 2 shows the kinetic-energy distributions for Ar_2^+ ions sampled from the same argon/oxygen plasmas. No structure is observed in these distributions because these ions are created by low-energy, three-body processes in the bulk of the plasma, and do not experience significant collisions as they transverse the sheath. As the oxygen content is increased, the maximum kinetic energies exhibit a trend similar to that observed for Ar^+. It is also evident from

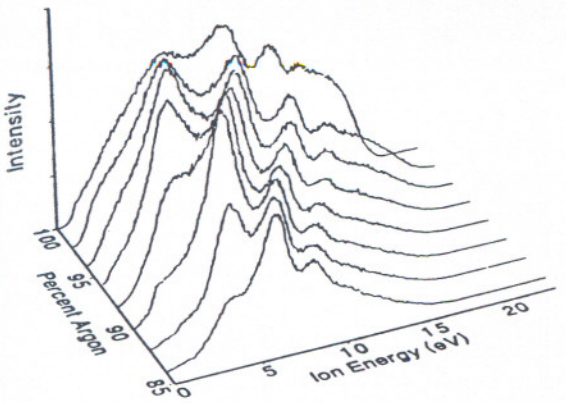

Figure 1. Ar^+ kinetic-energy distributions as a function of argon concentration in an argon/oxygen rf glow discharge. Oxygen concentrations range from 0 to 14%.

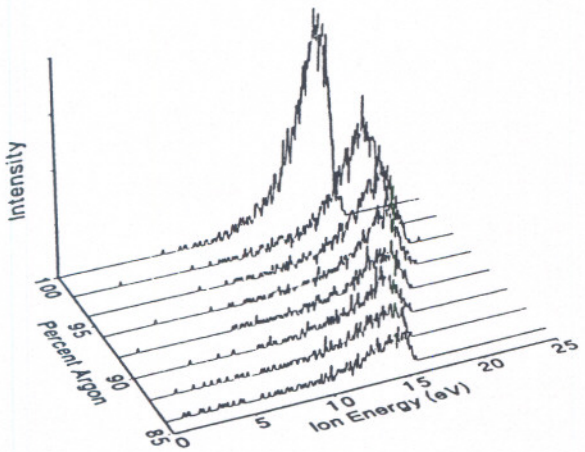

Figure 2. Ar_2^+ kinetic-energy distributions as a function of argon concentration in an argon/oxygen rf glow discharge. Oxygen concentrations range from 0 to 14%.

Fig. 2 that the intensity of the observed Ar_2^+ signal decreases with increasing oxygen content, but at a rate that is not proportional to the oxygen concentration. When the oxygen content is 14%, the intensity of the Ar_2^+ peak has been reduced by more than a factor of 7. This reduction in signal intensity cannot be explained by a simple dilution argument, and suggests that changes have occurred in the plasma that adversely affect the formation process, or that the mechanisms for the destruction of Ar_2^+ have become more significant as the oxygen content increases.

The kinetic-energy distributions for Ar^{++} are shown in Fig. 3. The distributions exhibit secondary maxima that are a result of Ar^{++} production in the sheath by high-energy electron collisions [8]. As the oxygen content changes, the Ar^{++} distributions exhibit energy shifts that are similar to those observed for Ar^+ and Ar_2^+. However, the most significant change is the decrease in observed signal intensity for the Ar^{++} ion as the oxygen content is increased from 0 to 2%. This 85% decrease in Ar^{++} intensity indicates a significant reduction in the number of high-energy electrons present in the discharge.

The kinetic-energy distributions for O_2^+ ions are shown in Fig. 4 for a series of argon/oxygen plasmas with oxygen concentrations ranging from 2–14%. For a 2% oxygen concentration, the O_2^+ kinetic-energy distribution is narrow and featureless, similar to the Ar_2^+ distributions in Fig. 2. This is due to the fact that, for low oxygen concentrations, most of the collisions experienced by the O_2^+ ions are with argon atoms, and the kinetic energy of the ions is not significantly affected by these collisions. Thus, since the O_2^+ ions are created primarily in the bulk plasma and since the kinetic energy of the ions are not significantly affected by collisions, the kinetic-energy distribution is representative of the average sheath potential experienced by the ion as it is accelerated toward the sampling cone. However, as the oxygen concentration increases, the number of O_2^+/O_2 collisions increase, and the large resonant charge-exchange cross section for oxygen [11] allows formation of O_2^+ ions that initially have "zero" (thermal) kinetic energies in the sheath. This affects significantly the measured kinetic-energy distributions for O_2^+ ions by causing broadening of the distribution and the formation of secondary maxima, similar to that observed for Ar^+.

Atomic oxygen ions, O^+, are also observed in discharges containing oxygen and are primarily formed by dissociative ionization of oxygen by high-energy electrons. Figure 5 shows kinetic-energy distributions for O^+ ions sampled from plasmas with the same range of oxygen concentrations as in Fig. 4. These distributions are broad and bimodal in nature, and exhibit only a minor dependence on the oxygen content. The bimodal structure indicates that O^+ is created in both the sheath and in the bulk region of the plasma. However, the O^+ kinetic-energy distributions do not exhibit the same type of secondary maxima that are apparent for other ions that are created in the sheath, such as O_2^+ (at higher oxygen concentrations), Ar^+, and Ar^{++}. This may be due to a "smearing out" effect that results from the fact that O^+ ions are created with significant initial kinetic energy in the dissociative ionization process [12].

It is also interesting to note that the intensities for O^+, like the ions produced from argon, do not scale with the oxygen concentration. However the intensity of the O_2^+ signal tracks the oxygen content quite closely.

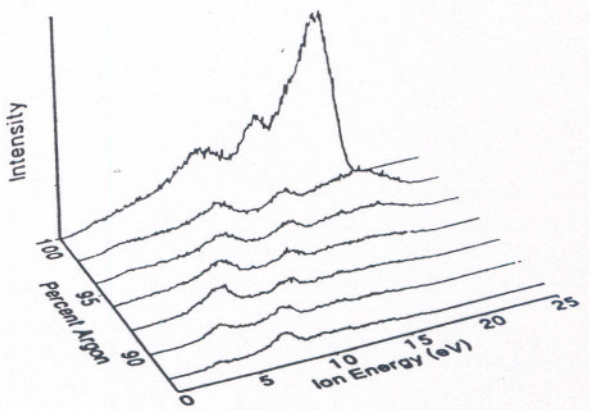

Figure 3. Ar^{++} kinetic-energy distributions as a function of argon concentration in an argon/oxygen rf glow discharge. Oxygen concentrations range from 0 to 14%.

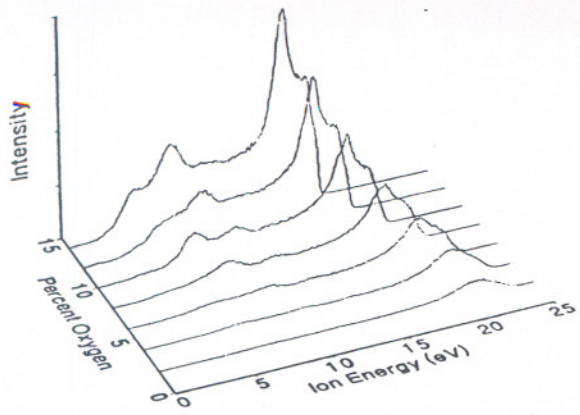

Figure 4. O_2^+ kinetic-energy distributions as a function of oxygen concentration in an argon/oxygen rf glow discharge.

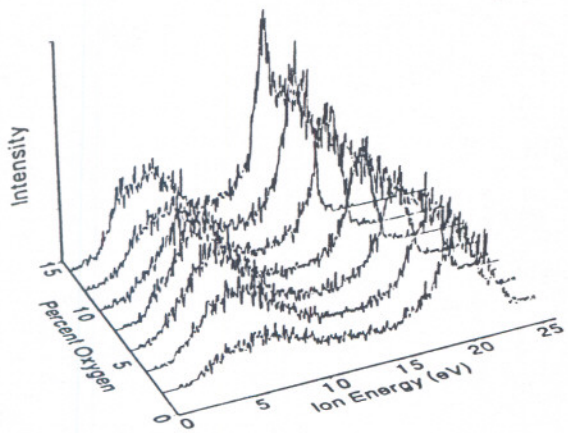

Figure 5. O^+ kinetic-energy distributions as a function of oxygen concentration in an argon/oxygen rf glow discharge.

Electrical Measurements

Figure 6 shows variations in plasma-related electrical parameters as a function of oxygen concentration. These electrical parameters were determined from voltage and current waveforms measured at the powered electrode simultaneously with the ion energy distributions presented in the previous section. The results of five waveform measurements were averaged. While the magnitudes and phases of the first five Fourier components were calculated for the current and voltage waveforms occurring across the plasma, only the values of the fundamental components are presented here. The magnitudes of the higher order voltage components were very small, accounting for less than 3% of the total measured voltage. The higher order current components had magnitudes ranging from 15 to 70 mA, and exhibited trends similar to those observed for the fundamental current component as the oxygen concentration was varied.

As the oxygen concentration increases from 0 to 20%, the fundamental voltage component across the plasma (V_1) exhibits a small decrease in amplitude, while the amplitude of the fundamental current component (I_1) decreases by 30%. The phase (ϕ_1) between V_1 and I_1 is observed to decrease by $\sim 9°$, in qualitative agreement with model calculations of electronegative plasmas [13]. The power dissipated in the plasma, as calculated from the measured waveforms, increased sightly with larger oxygen content.

The self-bias voltage (V_b) exhibits the most dramatic changes as the gas concentrations are varied. As the oxygen content is changed from 0 to 2%, V_b changes from −87.3 to −80.4 volts. A decrease in the absolute magnitude of the self-bias potential is expected because the formation of oxygen negative ions in the plasma has an equalizing effect on the positive and negative charge-carrier mobilities. It is seen, however, that the bias potential slowly increases as the oxygen concentration increases above 4%. The reason for this latter trend is not understood.

DISCUSSION

Previous work by Köhler *et al.* [14] indicates that the maximum kinetic energy observed in an energy distribution for a particular ion roughly corresponds to the average sheath potential that the

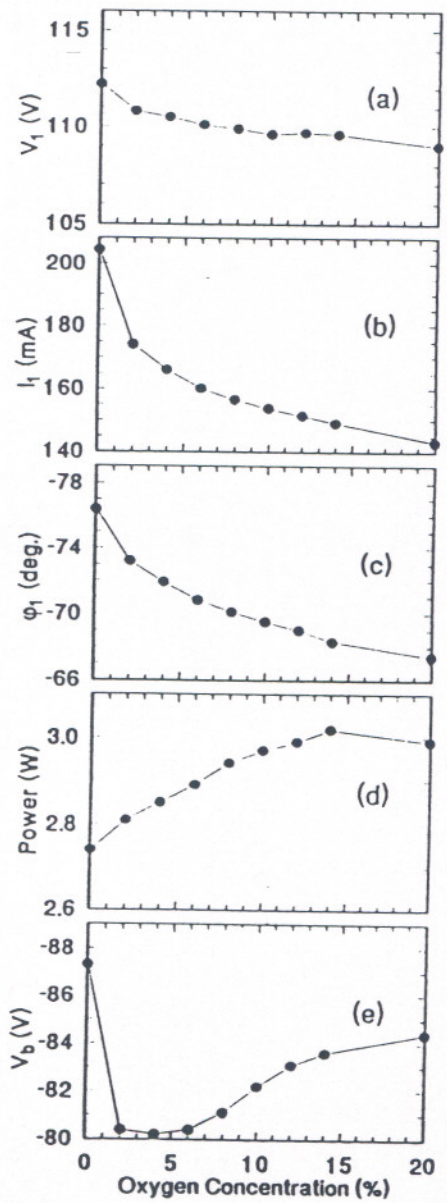

Figure 6. Plots of the (a) magnitude of the fundamental voltage component across the plasma, (b) the magnitude of the fundamental current component across the plasma, (c) the phase between V_1 and I_1, (d) the power dissipated in the plasma, and (e) the self-bias potential as a function of oxygen content in an argon/oxygen plasma. The total pressure was held constant at 13.3 Pa and the applied peak-to-peak rf voltage was 200 V for all experiments.

ion traverses before striking a surface. Figure 7 shows the maximum kinetic energies (energy at which the ion signal vanishes at the high-energy end of the distribution) from the distributions presented in Figs. 1-5 as a function of oxygen concentration. The maximum energies of Ar^+, Ar_2^+ and Ar^{++} are all grouped within about 1 eV of each other which is representative of the reproducibility of the measurements. The maximum energies of the O_2^+ ions lie slightly above the argon ions, perhaps due to less energy loss as the ions cross the sheath. The maximum energies for O^+ are 2 eV or more above those for argon ions.

A simple model of Köhler *et al.* [14] predicts the maximum kinetic energy (ϵ_{max}) of an ion traversing a sheath to be approximately

$$\epsilon_{max} \approx \frac{V_1 + V_b}{2}. \qquad (1)$$

Using the data from Figs. 6a and 6e, the results of Eq. (1) are shown in Fig. 7. While the values of ϵ_{max} predicted by Eq. (1) fall well below the measured values, the dependence upon oxygen concentration is in qualitative agreement, and shows a direct correlation between the electrical and ion-energy measurements. The differences in absolute magnitudes of ϵ_{max} may be explained by the fact that the simple model used to derive Eq. (1) ignores any resistive nature of the plasma and does not take into account the floating potential of the discharge. A detailed model is being developed to more accurately represent the discharge and to better predict the ion energies from electrical measurements. In addition, this discrepancy may also result from deficiencies in the model of stray impedance of the cell, which is used to calculate V_1. A more sophisticated treatment of the cell parasitics is being pursued [15].

Significant changes are observed in all of the electrical parameters and in the kinetic-energy distributions as the oxygen content of the plasma feed gas is increased. The largest incremental changes for all of the data occur between the 0 and 2% oxygen concentrations. These changes are most evident in the measurements of V_b, I_1, V_1, and in the observed increases in maximum kinetic energies for Ar^+, Ar_2^+, and Ar^{++}. The dramatic nature of these changes caused by adding small amounts of O_2 to an argon discharge indicates the importance of understanding more fully the effects of electronegative gases and gas-phase impurities on plasma conditions.

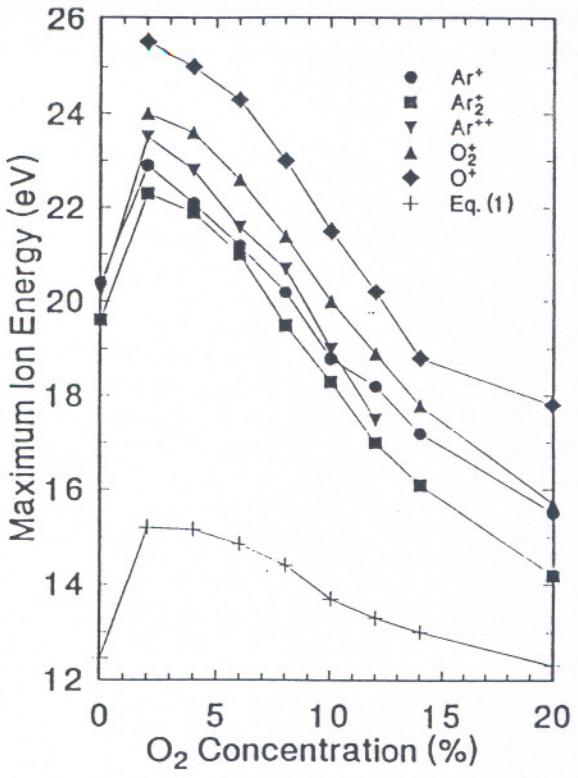

Figure 7. Plot of maximum ion kinetic energies from Figs. 1-5 and from Eq. (1).

ACKNOWLEDGEMENT

This work was performed in the Electricity Division of the Electronics and Electrical Engineering Laboratory, and in the Process Measurements Division of the Chemical Science and Technology Laboratory, National Institute of Standards and Technology, Technology Administration, U. S. Department of Commerce.

REFERENCES

1. Overzet, L. J., Beberman, J. H., and Verdeyen, J. T., 1989, *J. Appl. Phys.*, **66**, 1622.

2. Olthoff, J. K., Roberts, J. R., Van Brunt, R. J., Whetstone, J. R., Sobolewski, M. A., Djurovic, S., 1992, *Process Module Metrology, Control, and Clustering*, SPIE **1594**, pp. 168–178.

3. Roberts, J. R., Olthoff, J. K., Van Brunt, R. J., and Whetstone, J. R.,1991, *Advanced Techniques for Integrated Circuit Processing*, SPIE **1392**, pp. 428–436.

4. Hargis, P. J., Gerado, J. B., Greenberg, J. B., Miller, P. A., Torczynski, J. R., Sobolewski, M. A., Roberts, J. R., Olthoff, J. K., Whetstone, J. R., Van Brunt, R. J., Anderson, H. M., Mock, J. L., Splichal, M., Bletzinger, P., Garscadden, A., Gottscho, R. A., Selwyn, G., Butterbaugh, J. W., Dalvie, M., Brake, M. L., Passow, M. L., Elta, M. E., Graves, D. B., Swain, H. H., Kushner, M. J., Verdeyen, J. T., Horwath, R., and Turner, T. R., 1992, *Rev. Sci. Instrum.*, submitted.

5. Miller, P. A., Anderson, H., and Spichal, M. P., 1992, *J. Appl. Phys.* **71**, pp. 1171–1175.

6. The identification of commercial materials and their sources is made to describe the experiment adequately. In no case does this identification imply recommendation by the National Institute of Standards and Technology, nor does it imply that the instrument is the best available.

7. Sor-el, H. Z., 1967, *Rev. Sci. Instrum.*, **38**, pp. 1210.

8. Olthoff, J. K., Van Brunt, R. J., Radovanov, S., 1992, *J. Appl. Phys.*, submitted.

9. Wild, C., and Koidl, P., 1991, *J. Appl. Phys.* **69**, pp. 1253.

10. Liu, J., Huppert, G. L., and Sawin, H. H., 1990, *J. Appl. Phys.*, **68**, pp. 3916.

11. Stebbings, R. F., Turner, B. R., and Smith, A. C. H., 1963, *J. Chem. Phys.*, **38**, pp. 2277.

12. Van Brunt, R. J., Lawrence, G. M., Kieffer, L. J., and Slater, J. M., 1974, *J. Chem. Phys.*, **61**, pp. 2032–2037.

13. Makabe, T., 1992, *Gaseous Electronics and Its Applications* (KTK Scientific Publishers, Tokyo), pp. 236–273.

14. Köhler, K., Coburn, J. W., Horne, D. E., and Kay, E., 1985, *J. Appl. Phys.*, **57**, pp. 59–66.

15. Sobolewski, M. A., in preparation.